Low-speed Airfoil Design and Synthesis with the Cubic Spline

J. Philip Barnes, March 2010

INTRODUCTION

In this article, we highlight a new and powerful method for low-speed airfoil design and synthesis. Our motivation is to offer more simplified, and yet more powerful, methods to define and synthesize low-speed airfoil geometry and to calculate pressure and viscous forces and moments (this article limited to inviscid flow).

We'll leverage the power of the cubic spline, together with a new formulation, to first define an airfoil with just one "spline knot" on each upper and lower surface. Then adding a few more points, we can obtain a compact, smooth, and accurate model of any airfoil. In calculating surface pressures with the well-known vortex-panel method, we'll introduce new and fundamental methods which "slay the dragon of discontinuity" when it becomes necessary to compute the panel-self-induced normal and tangential velocities. Finally the new methods, once reasonably validated with test data, are applied toward the design of an efficient, high-lift laminar airfoil.

1.0 AIRFOIL GEOMETRY DEFINITION

Traditionally, airfoil geometry has been defined by a lengthy tabulation of coordinates, (z/c) versus (x/c). Typically, 70 or so points are necessary to mitigate both the differences in interpolation methods and the risk of oscillations in computed velocity near the leading edge.

An efficient and ultimately more accurate alternative is to characterize the geometry with a handful of well-placed points, then interpolating between points with a spline. Choices then become the type of spline and the type of coordinates. Herein we apply a *cubic spline* together with the *Glauert Coordinate*, the latter representing the polar angle (ϕ) taken clockwise from the lower trailing edge. This approach enjoys "automatic" anchor points at the leading and trailing edges, enabling airfoil construction with as little as one "spline knot" on each upper/lower surface (Figure 1.0-1). For any number of knots, this approach ensures continuous curvature throughout, including the leading edge where such continuity is particularly important. EQ [1.0-1] relates the horizontal coordinate ($X \equiv x/c$) and Glauert coordinate, the latter used for cubic-spline interpolation of the vertical coordinate ($Z \equiv z/c$) as shown in Figure 1.0-2.

$$X \equiv x/c = (1/2)\,(1 + \cos\phi) \qquad [1.0\text{-}1]$$

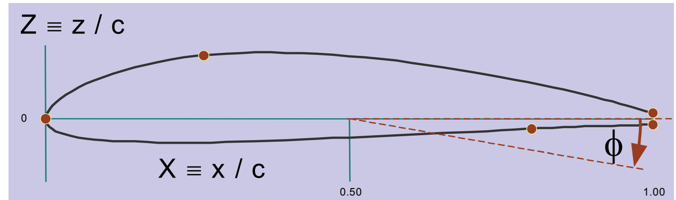

Figure 1.0-1 "One-point-per-surface" Airfoil

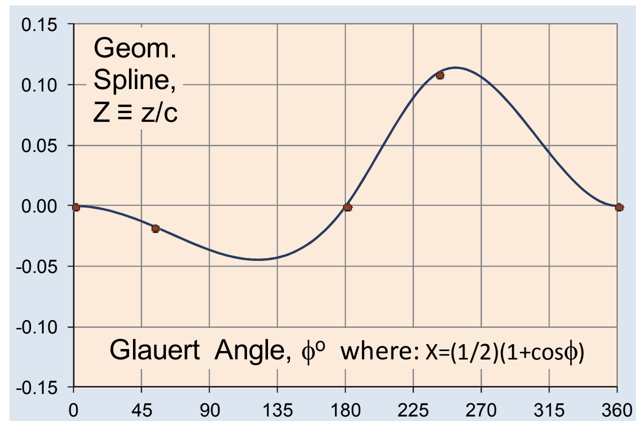

Figure 1.0-2 Spline-based Geometry Characterization

2.0 CUBIC SPLINE REVIEW AND RENEW

The cubic spline numerical method joins a series of "knots," each having coordinates (X,Y), with a series of third-order polynomials, while preserving continuity of the zeroth, first, and second derivatives at each *internal* knot. Although with this method the third derivative is in general not continuous, indeed exhibiting a "zig-zag" shape, we postulate that airfoil geometry characterized with a cubic spline will be in effect smooth, not only to the eye, but also to the air flowing over it.

3.0 PANEL-METHOD OVERVIEW

Our linear-vortex-panel method follows the general approach of Katz and Plotkin (3), but with a different approach to calculate panel-to-panel and self-induced velocities, accommodation of panel curvature, and mixed (normal versus tangential) boundary conditions.

Our objective is to solve for the distribution of pressure coefficient (c_p) and velocity along the airfoil surface in inviscid, low-speed flow. Although such modeling is "inviscid," viscosity is in fact essential for the development of lift by giving rise to the boundary layer and by enforcing the well-known *Kutta Condition* at the trailing edge.

The boundary layer is herein modeled as an infinitely-thin continuous vortex surface with local vortex density (γ), the latter positive when rotating clockwise for "left-to-right" flow. Airfoil geometry and vortex density are non-dimensionalized, respectively, to the chord (c) and flight velocity (v_o). The non-dimensional distance ($S \equiv s/c$) is integrated beginning at the lower trailing edge, including the effects of local curvature, as unit normal vectors (**n**) are computed. Applying boundary conditions, with self-induced velocities where applicable, we solve for the non-dimensional vortex strength ($G \equiv \gamma/v_o$) at (n_v) vortex cores.

3.1 SPLINE-BASED VECTOR INTEGRATION

In Figure 3.1-1, the incremental sub vortex ($\gamma_k\ \Delta s$) induces a velocity [$v_{ik} = \gamma_k \Delta s\ /\ (2\pi r_{ik})$] at node (i), the latter having unit normal and tangential vectors ($\mathbf{n}_i$) and ($\mathbf{t}_i$), respectively. In general, we apply the boundary condition whereby the velocity normal to the surface at node (i) is zero, and where such normal velocity is the vector sum thereof induced by the free stream and the vortex surface. With the aid of a cubic spline, vectors, and new methods herein for self-induced velocities, we integrate over the vortex surface for the non-dimensional normal velocity (ν_i) at each node (i). To avoid numerical difficulties near the trailing edge, we apply the *tangential* counterpart of this boundary condition.

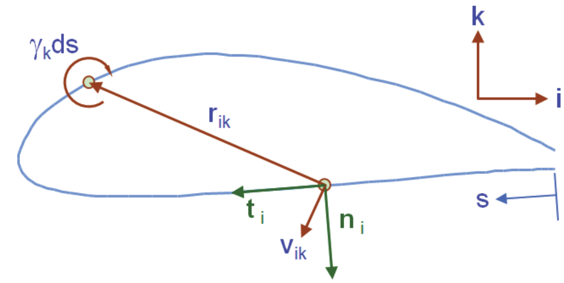

Figure 3.1-1 Induced Velocity Vector Integrand Constituents

3.2 PANEL-SELF-INDUCED NORMAL VELOCITY

At the center of panel (a-b) in Figure 3.2-1, we now compute the panel-self-induced normal velocity. The simplest study treats the panel as flat, but it can be shown that a fixed radius of curvature will have no effect. First, we characterize the local non-dimensional vortex density ($G=\gamma/v_o$) as parabolic with non-dimensional distance (S) from the panel center. G(S) is then distilled to three isolated components representing the average, first derivative, and second derivative. By inspection, the effects of the average cancel. Also, paying careful attention to sign, we discover that the effects of the 2nd-derivative also cancel, whereby we need concern ourselves only with the 1st derivative (dG/dS), given by [$(G_b-G_a)/(S_b-S_a)$].

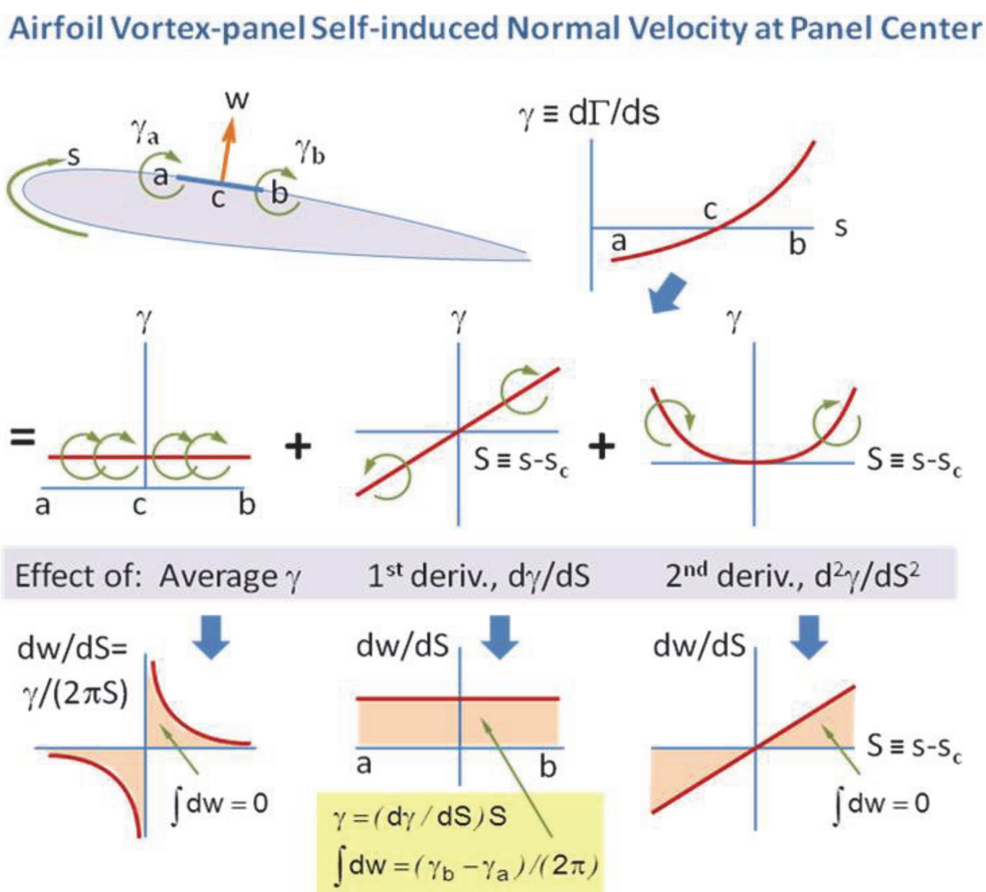

Figure 3.2-1 Self-induced Normal Velocity Study

3.3 SELF-INDUCED TANGENTIAL VELOCITY

When integrating induced *normal* velocity, we find that the strong mutual influence of upper and lower panels adjacent to the trailing edge leads to relatively large integrands together with mid-panel sign changes. These phenomena locally de-stabilize the solution for vortex strength. An alternative boundary condition, based on the *tangential* induced velocity, essentially resolves this problem. As before, however, we encounter the need to compute panel-self-induced velocity when integrating effects of the vortex surface.

Assuming the vortex panel is flat, a first look suggests that the panel-self-induced tangential velocity is either zero or perhaps undefined. However, taking into consideration the finite thickness of the boundary layer, while recognizing that the local velocity of interest resides just outside the boundary layer, we find that the self-induced tangential velocity is not zero. Figure 3.3-1 derives the self-induced tangential velocity increment (dv_t) which, integrated in the limit as the b'layer thins, yields the self-induced tangential velocity of EQ 3.3-1.

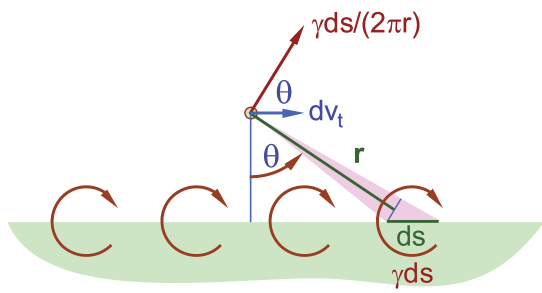

Figure 3.3-1 Panel Self-induced Tangential Velocity Study

$$\Delta\tau_{ii} \equiv \frac{\Delta v_t}{v_o} = \frac{2}{v_o}\int_o^{\pi/2} \frac{\gamma_i\, ds}{2\pi r}\cos\theta$$

$$= \frac{2}{v_o}\int_o^{\pi/2} \frac{\gamma_i\, ds}{2\pi r}\frac{r\, d\theta}{ds} = \frac{2}{v_o}\frac{\gamma_i}{2\pi}\int_o^{\pi/2} d\theta$$

$$= \frac{\gamma_i}{2v_o} = G_i / 2 \qquad [3.3-1]$$

A similar analysis to that carried out for the normal velocity reveals for tangential velocity that the effects of (G'=dG/dS) cancel, whereas the effects of both the average and 2^{nd}-derivative remain. However, we will assume herein that the effects of the 2^{nd}-derivative on panel self-induced tangential velocity near the trailing edge can reasonably be neglected. To end this section, we note that a reasonable solution can be obtained applying the tangential boundary condition throughout, but at some expense in "numerical stiffness."

3.4 METHOD VALIDATION

The method obtains a good match with test data as shown for three airfoils in Figures 3.4-1 though 3.4-3, the first three sub-figures representing the geometry spline, vortex density, and pressure coefficient of the FX66 airfoil. Recall that the magnitude |G| is the ratio of local-to-flight velocity. For example, we see that the maximum upper-surface velocity is 60% greater than flight velocity. Looking more closely, we observe the stagnation point (G=0) to reside on the lower surface at about 0.5% of chord aft of the leading edge At the trailing edge, the airflow slows down to 85% of flight velocity. With further inspection, we notice upper-surface laminar-to-turbulent transition at 48% chord (62% lower surface). By plotting either (G) or ($1-c_p$) versus (X), the upper surface naturally resides on top, without the need for scale inversion.

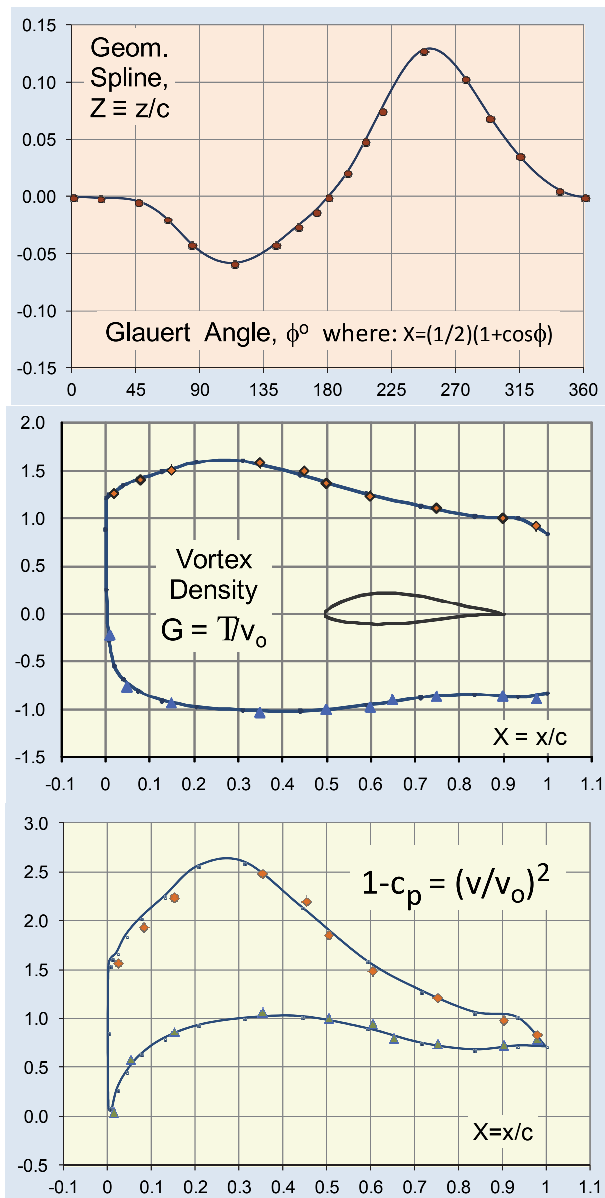

Figure 3.4-1 Method Validation, FX66 Airfoil, $\alpha=4^o$

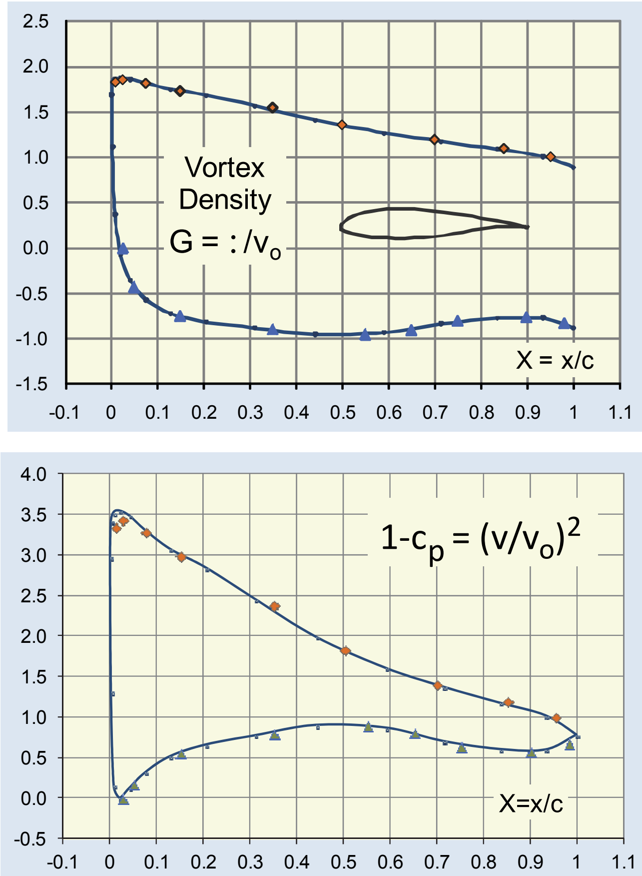

Figure 3.4-2 Method Validation, NLF(1)-0416 Airfoil, $\alpha=8^{o}$

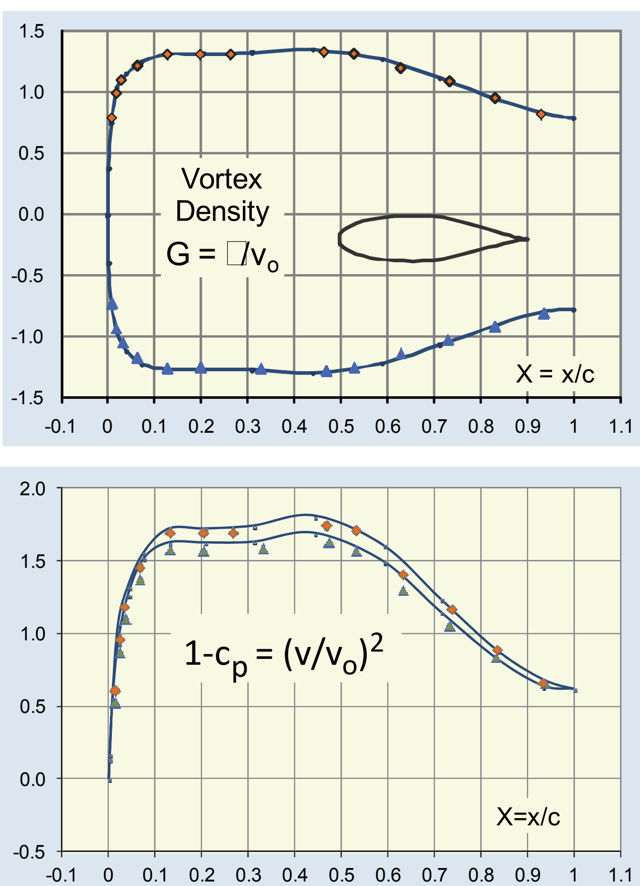

Figure 3.4-3 Method Validation, NACA 45-125 Airfoil, $\alpha=0^{o}$

4.0 METHOD APPLICATION

We now apply the methods herein to obtain the PCS-001 laminar airfoil of Figure 4.1. Defined by 13 spline knots, it has the popular "laminar rooftop" feature for high lift and low drag. Selected knots on the upper forward surface were manually adjusted to get the "plateau" represented by constant pressure and constant velocity. Not yet knowing its stall characteristics, further analysis and testing are needed to assess its suitability for safe flight.

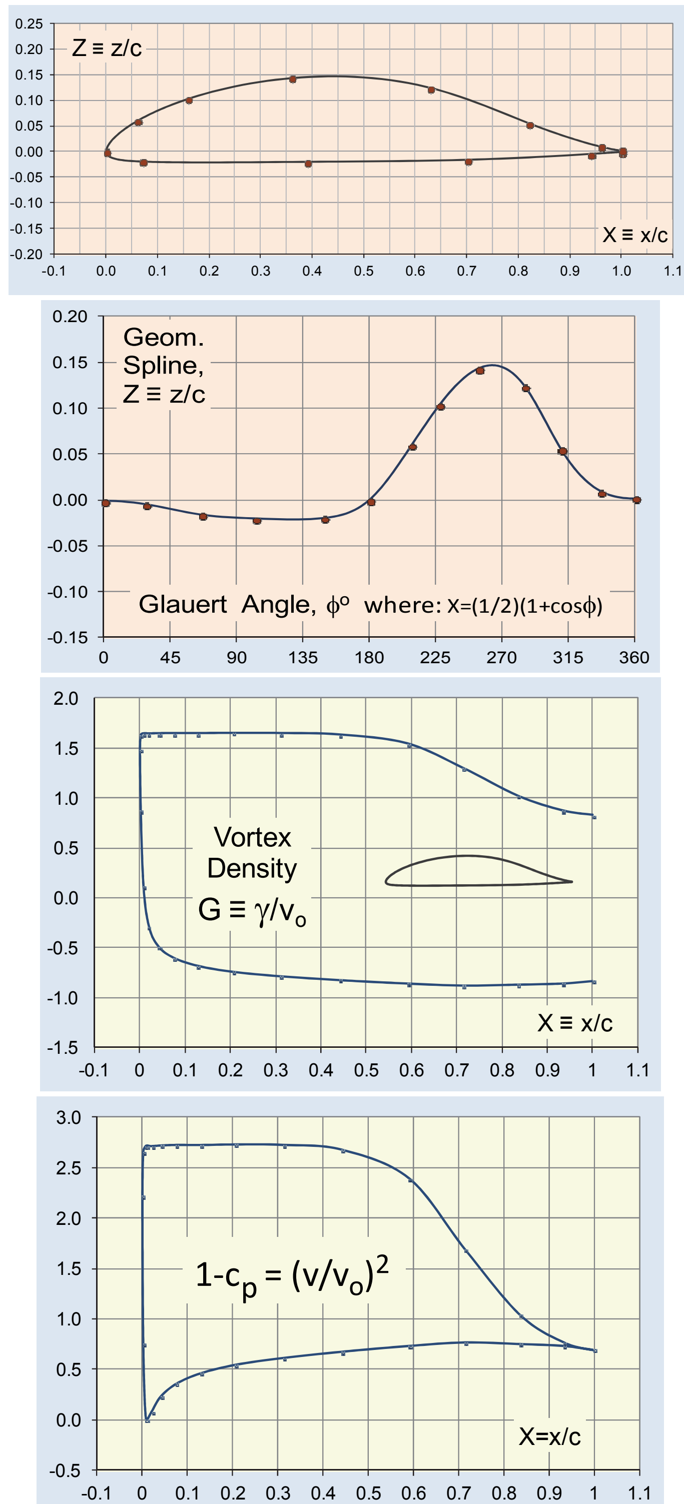

Figure 4.1 PCS-001 Laminar Airfoil, $\alpha=6.9^{o}$